Ceramics International 48 (2022) 10328–10332

Contents lists available at ScienceDirect

Ceramics International

journal homepage: www.elsevier.com/locate/ceramint

Enhanced dielectric and ferroelectric responses in La^{3+}/Ti^{4+} co-substituted $SrBi_2Ta_2O_9$ Aurivillius phase

Zulhadjri *, Tio Putra Wendari, Mukhniyal Ikhram, Yulia Eka Putri, Upita Septiani, Imelda

Department of Chemistry, Faculty of Mathematics and Natural Sciences, Universitas Andalas, Kampus Limau Manis, Padang, 25163, Indonesia

ARTICLE INFO

Keywords:
Aurivillius
Cations substitution
Orthorhombic structure
Dielectric constant
Ferroelectric behavior
Diffused phase transition

ABSTRACT

The molten salt technique was employed to prepare the Aurivillius phases $SrBi_2Ta_2O_9$ (SBT) and $Sr_{0.9}La_{0.1}Bi_2Ta_{1.9}Ti_{0.1}O_9$ (SLBTT). The XRD data and the Le Bail refinement approach demonstrate that both samples formed the double-layer Aurivillius phase with the orthorhombic $A2_1am$ structure successfully. The SLBTT cell volume is smaller compared to SBT with the substitution of smaller La^{3+} and Ti^{4+} ions and the increased size of the plate-like grains. FTIR analysis indicates the two local arrangements of Ti^{4+} at the *B*-site to form Ti–O–Ti and Ti–O–Ta bonds. Changes in the structural properties due to La^{3+} and Ti^{4+} substitution are reflected in the electrical properties. The higher ferroelectric transition temperature (T_c) of 455°C with the diffused phase transition behavior (DPT) was obtained in SLBTT. The unsaturated hysteresis loop of SLBTT obtained the ferroelectric remnant polarization (P_r) of 0.43 μC/cm^2 and the coercive field (E_c) of 110.6 kV/cm, respectively. The enhanced ferroelectric characteristic as well as a higher bandgap (E_g) that is driven by the substitution of variable smaller cations.

1. Introduction

Recently, the ferroelectric materials have been an exciting subject of intense research due to their potential applications in electronic devices, non-volatile ferroelectric random-access memory, energy storage, piezoelectric generator, electrocaloric, solar cell, and etc. [1–5]. The Aurivillius compound is composed of a bismuth layer $[Bi_2O_2]^{2+}$ and a perovskite layer $[A_{m-1}B_mO_{3m+1}]^{2-}$ whereby m represents the number of Aurivillius layers [6]. Here, the $(Bi_2O_2)^{2+}$ layers play a crucial role in space-charge compensation and insulation of the materials as well as the perovskite-like layers with d^0-configuration cations and the distorted BO_6 octahedra give rise to high electrical polarization, resulting in the ferroelectric behavior in nature with a high transition temperature (T_c). The double-layer Aurivillius $SrBi_2Ta_2O_9$ ($m = 2$) show excellent ferroelectric properties with a Curie temperature (355 °C), low leakage current, and fatigue resistance [7].

Numerous reports are available on the enhancement of the electrical properties of Aurivillius compounds with a suitable compositional modification. A common approach is the substitution of lanthanide ions (Ln^{3+}) on *A*-site, and has reported the enhancement of piezoelectric and ferroelectric characteristics by suppressing the formation of oxygen vacancies and reducing the leakage current in Aurivillius compounds [8–11]. Additionally, substitution transition metal ions with d^0-configuration on *B*-site offer the improved ferroelectric properties [12,13]. As a result, the perovskite layer was shown to be highly amenable to cation substitution at the *A*-site, the *B*-site or both, resulting in enhanced electrical characteristics as well as inducing the transition from a normal ferroelectric to a relaxor-ferroelectric.

In this work, the double-layer Aurivillius compound $SrBi_2Ta_2O_9$ was simultaneously substituted by the La^{3+} for Sr^{2+} at the *A*-site and Ti^{4+} for Ta^{5+} at the *B*-site to obtain charge neutrality and also oxygen content constant. We have synthesized the $SrBi_2Ta_2O_9$ (SBT) and $Sr_{0.9}La_{0.1}Bi_2Ta_{1.9}Ti_{0.1}O_9$ (SLBTT) compounds using the molten salt technique that has not previously been reported. The structure, morphologies, dielectric, and optical properties of both compounds were systemically studied.

2. Experimental procedures

$SrBi_2Ta_2O_9$ (SBT) and $Sr_{0.9}La_{0.1}Bi_2Ta_{1.9}Ti_{0.1}O_9$ (SLBTT) samples were synthesized by the molten salt technique using the sulfate salt fluxes. The stoichiometric molar ratio of Bi_2O_3, $SrCO_3$, La_2O_3, TiO_2, and Ta_2O_5 (Aldrich, ≥ 99.9%) was mixed with K_2SO_4/Na_2SO_4 salts with a mole ratio of 1:7, and then ground in an agate mortar for 2 h. The

* Corresponding author.
E-mail address: zulhadjri@sci.unand.ac.id (Zulhadjri).

https://doi.org/10.1016/j.ceramint.2022.01.307
Received 29 October 2021; Received in revised form 22 January 2022; Accepted 27 January 2022
Available online 3 February 2022

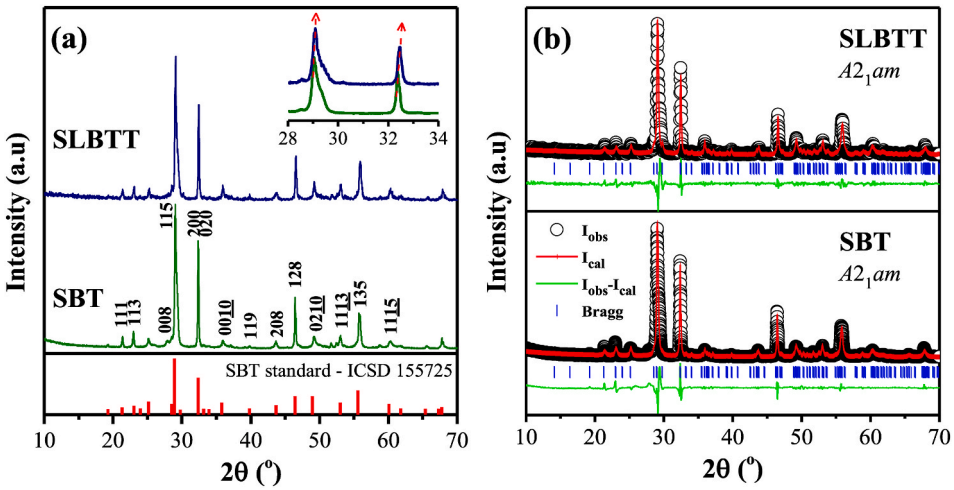

Fig. 1. (a) XRD patterns; (b) Le Bail refinement plots to XRD data of the SBT and SLBTTO samples.

mixtures were heated at 750 °C for 10 h, 850 °C for 5 h, and 950 °C for 5 h with intermediate grinding steps after each heating stage. The product was then washed with hot distilled water for sulfate fluxes removal, and then dried at 110 °C for 12 h. The phase formation was analyzed by X-ray diffraction (XRD; PANalytical). The structural parameters were determined by the Le Bail refinement technique using the RIETICA software [14]. FTIR spectroscopy (Shimadzu IRPrestige21) was carried out to inspect the vibrational mode of the bond, and the surface morphology was studied using a Scanning Electron Microscope (SEM; INSPECT S50). Regarding electrical measurement, the powder was mixed with 5% *wt* PVA as a binder and pressed into pellets. The pellets were heated at 550 °C for 3 h for burning out the PVA, and then sintered at 950 °C for 5 h. The sintered pellets were electroded with silver paste (Aldrich, 99%), and dried at 130 °C for 2 h. The dielectric characteristics were measured with an LCR-meter (BK Precision) in the range of 50 kHz–300 kHz, as a function of temperature. A modified Sawyer–Tower circuit at room temperature measured the ferroelectric *P-E* hysteresis loops applying a maximum electric field of 190 kV/cm with a frequency of 100 Hz [15]. The optical bandgap was investigated by the UV–Vis Diffuse Reflectance Spectroscopy (UV-DRS; SPECORD 210).

3. Results and discussion

Fig. 1a depicts the XRD patterns of the SBT and SLBTTO. The XRD peaks were properly indexed with the standard data of $SrBi_2Ta_2O_9$, with an orthorhombic $A2_1am$ structure (ICSD #155725), thus confirming the formation of double-layer Aurivillius phase. It is worthy to note that the presence of the most intense XRD peak of (115), coinciding with the (112m+1) peak in the Aurivillius phases [12]. This corresponds to the number of layers (m = 2). Furthermore, the enlarged XRD patterns indicate that the diffraction peaks of the SLBTTO slightly shift to higher 2θ, indicating a decreased cell volume because of the introduction of La^{3+} and Ti^{4+} cations.

Using the Le Bail refinement approach, the refinement fits for the XRD data with the orthorhombic space group $A2_1am$ are depicted in Fig. 1b. The refinement plots indicate good fits between the observed XRD patterns and the calculated patterns; this confirms the formation of the double-layer Aurivillius phase with an orthorhombic $A2_1am$ structure [16]. The refined lattice parameters of SBT are as follows: a = 5.5251(5) Å; b = 5.5215(8) Å; c = 25.016(5) Å; V = 763.02(8) Å^3, and SLBTT are a = 5.5126(1) Å; b = 5.5153(3) Å; c = 25.01(2) Å; V = 760.185(1) Å^3. The lattice parameters and cell volume of SLBTT are shown to be smaller, primarily due to the substitution of smaller La^{3+} (1.36 Å) for Sr^{2+} (1.44 Å), as well as smaller Ti^{4+} (0.605 Å) for Ta^{5+} (0.64 Å) [17]. Additionally, the decreased cell volume can alter the BO_6 octahedra in the *ab*-plane, and consequently the SLBTT structure becomes more orthorhombic, as quantified by the higher orthorhombicity ratio [(*a*-*b*)/(*a*+*b*)] of SLBTT (0.00043) compared to SBT (0.00032).

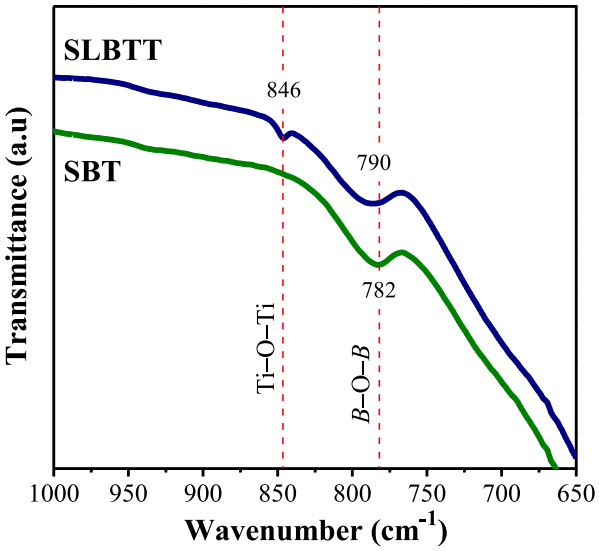

Fig. 2. FTIR spectra of SBT and SLBTTO samples at room temperature.

The FTIR spectra in Fig. 2 depicts a vibration mode of SBT at ~782 cm^{-1}, coinciding with the asymmetric *B*–O stretching vibration of the BO_6 octahedra. This mode is seen to have a minor change to a higher wavenumber of ~790 cm^{-1} for SLBTT. Remarkably, a new vibration mode at ~846 cm^{-1} was seen within the SLBTT. These results indicate the potential arrangement of substituted Ti^{4+} ions on the *B*-site perovskite layers. This shifting mode indicates that Ti^{4+} ions distribute among Ta^{5+} to form Ti-O-Ta arrangements, because Ti^{4+} have a smaller ionic mass (47.86 amu) as compared to Ta^{5+} (180.94 amu) [18,19]. Also, the Ti^{4+} ions also form a locally ordered Ti–O–Ti arrangement since the ~846 cm^{-1} mode is shown when Ti^{4+} ions are introduced to the SBT structure. The local order of transition ion on the *B*-site perovskite has also been shown in prior work [20].

SEM micrographs in Fig. 3 demonstrate the anisotropic plate-like grains, which is a prominent feature of the Aurivillius phase. This plate-like grain was formed owing to the high grain growth rate in the direction perpendicular to the *c*-axis caused by the lower surface

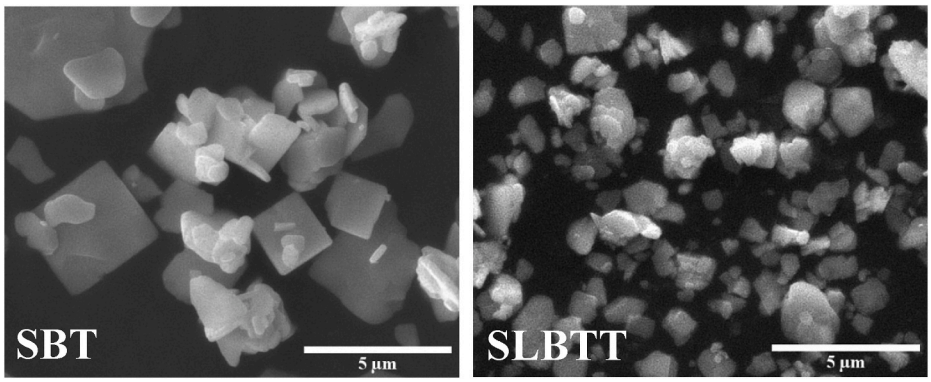

Fig. 3. SEM micrograph of the powder samples.

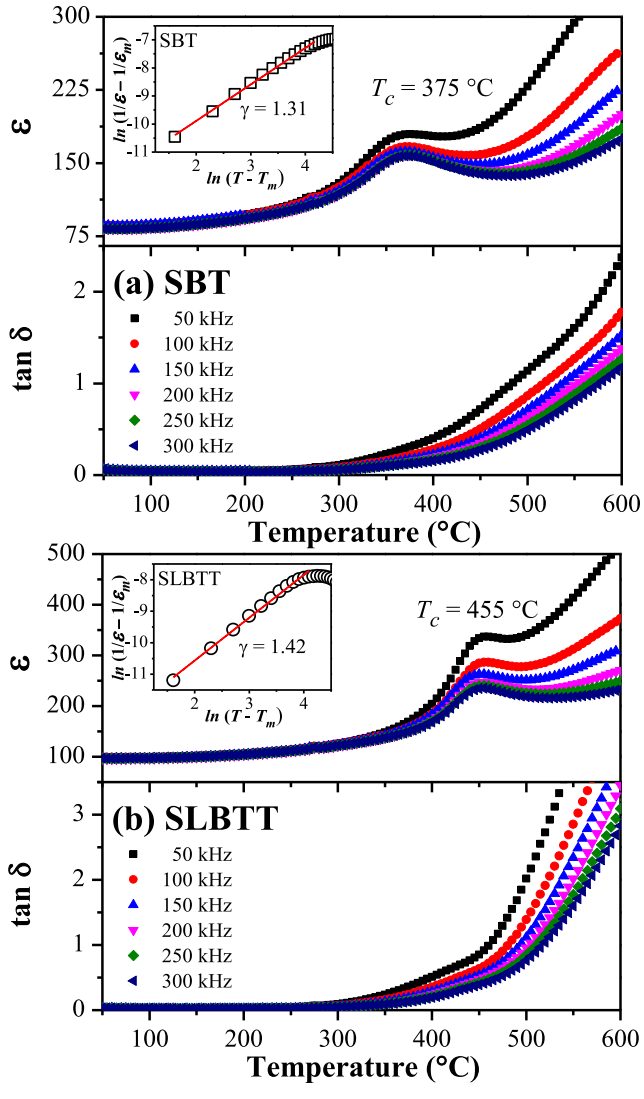

Fig. 4. Temperature dependence of SBT and SLBTT dielectric constants and loss.

energies of the (001) planes induced primarily during sintering [18]. The grain size of SLBTTO is within 0.3–1.5 μm, which is much smaller compared to SBT with the size of 0.4–3.3 μm since La^{3+} ions inhibit the grain growth [16].

The dielectric constant (ϵ) and dielectric loss (tan δ) are plotted against temperature measured at different frequencies of 50–300 kHz and are shown in Fig. 4. The high-frequency dielectric measurement yields a drastic reduction in the contribution of the leakage current density as the extrinsic factor on the ferroelectric polarization. Therefore, the magnitude of dielectric constant accurately represents the effect of structural distortion as the intrinsic factor contributing to the ferroelectric properties [21]. A dielectric peak was observed at 375 °C for SBT, and at a higher temperature of 455 °C for SLBTT, thus corresponding to the ferroelectric transition temperature (T_c) [22]. SLBTT also demonstrated a higher magnitude of dielectric constant at both room temperature (RT) and T_c (see Table 1). These results are in line with the more altered orthorhombic structure of SLBTT, as mentioned in refinement analysis. The increase in structural distortion is significantly impacted by the substitution of smaller La^{3+} and Ti^{4+} ions, hence the higher T_c [23]. Additionally, the tan δ values of both samples were seen to be low in temperature below T_c, indicating the high thermal stability. The higher value of ϵ at room temperature and high temperature at high frequency makes the SLBTT sample a suitable candidate for high-temperature and high-frequency applications.

Table 1
Value of electrical properties of SBT and SLBTT measured at 300 kHz.

Sample	T_c	ϵ_m (T_c)	tan δ (T_c)	ϵ (RT)	tan δ (RT)	γ
SBT	375 °C	157.5	0.125	86.3	0.096	1.31
SLBTT	455 °C	234.8	0.411	96.3	0.034	1.42

Furthermore, both samples show the broad peak of dielectric constant but does not exhibit the frequency-dispersive behavior. Typically, this phenomenon is preferably known as the diffused ferroelectric phase transition (DPT) behavior [16,24,25]. The diffuseness of the phase transition (γ) can be evaluated by the linear fitting of the modified Curie-Weiss curve, as seen in the inset of Fig. 4 [9]. SLBTT shows a higher γ value (1.42) compared to SBT (1.31), attributed to the DPT behavior of both samples. DPT behavior is generally attributed to perovskites when at least two different cations occupy the same crystallographic site. DPT behavior in SBT might be attributed to the disorder of Sr^{2+} and Bi^{3+} in the Bi_2O_2 layers, which has also been confirmed using a combination of X-ray and neutron powder diffraction [26]. Thus, a more pronounced DPT behavior of SLBTT was induced by the higher disorder of the *A*-site cations (Sr^{2+}/Bi^{3+}/La^{3+}) and *B*-site cations (Ta^{5+}/Ti^{4+}) within the Bi_2O_2 and perovskite layers [22]. The simultaneous substitution is found to induce chemical and structural inhomogeneity that leads to structural disorder reflected as increasing diffuseness in the transition.

Since SBT and SLBTT samples show a transition temperature of ferroelectric, polarization-electric field (*P-E*) hysteresis loops were measured at RT and 100 Hz, as shown in Fig. 5. It is noticed that the *P-E* loops of both samples are unsaturated, implying that the domains are not fully aligned at the maximum applied electric fields of 190 kV/cm.

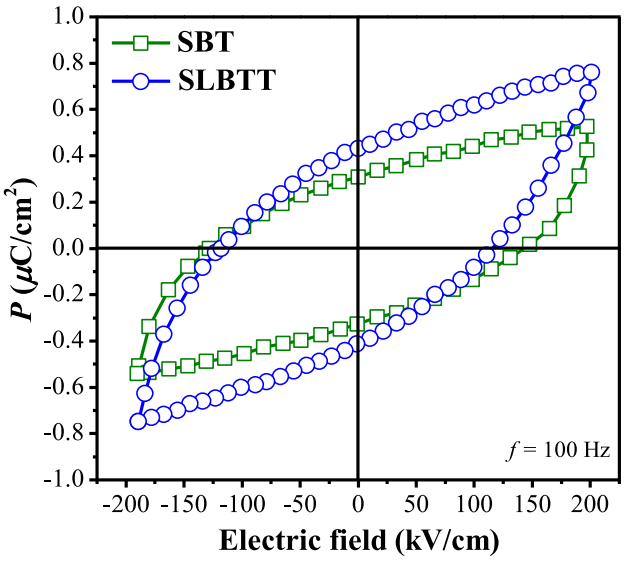

Fig. 5. *P-E* hysteresis loops of SBT and SLBTT measured at room temperature and 100 Hz frequency.

Although unsaturated, both samples adopt the typical non-linear hysteresis with opening loops, indicating the ferroelectric behavior at RT [8,27]. The measured remanent polarization (P_r) and the coercive field (E_c) values of the SBT are about 0.31 μC/cm^2 and 128.2 kV/cm, respectively. Clearly, the substitution of La^{3+} and Ti^{4+} ions in SLBTT results in the enhanced ferroelectric properties with higher P_r of 0.43 μC/cm^2 and lower E_c of 110.6 kV/cm. These results are coincided with the increase in both T_c and ϵ (see also Table 1), which originates from the higher structural distortion.

The bandgap (E_g) of Aurivillius samples was measured from the intersecting point of the linear fits by the curve $(F(R\infty)h\upsilon)^2$ versus $h\upsilon$ [4], as illustrated in Fig. 6. The approximate E_g value of SBT is 2.81 eV, and this increases for SLBTT to 2.86 eV, which is related to the structural distortion effect [16]. Previous works found that the decreased size of the *A*-site cations results in higher E_g energy within the perovskite-structured compounds [23,28]. Thus, the substitution of smaller La^{3+} on *A*-site perovskite layer causes a shift of the valence band to higher energy, and induces larger E_g. It is also evident by the higher dielectric constant and lower tan δ at RT (see Table 1) because of the decline in charge conduction that is caused by the broader E_g.

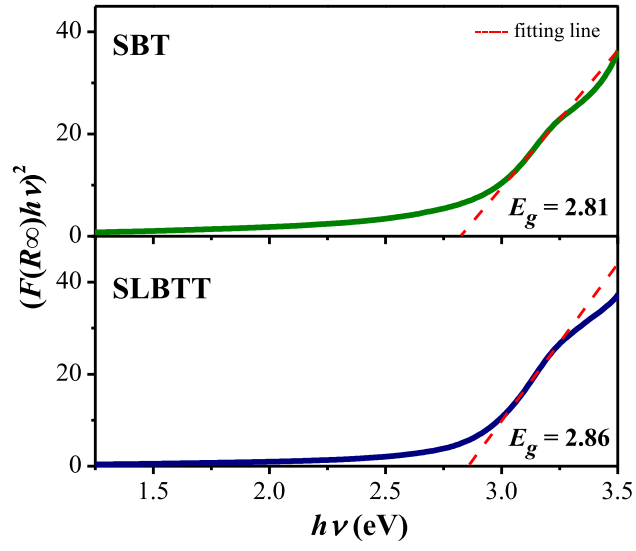

Fig. 6. $(F(R\infty)h\upsilon)^2$ plots as a photo energy ($h\upsilon$) function for the identification of E_g.

4. Conclusions

In summary, $SrBi_2Ta_2O_9$ (SBT) and $Sr_{0.9}La_{0.1}Bi_2Ta_{1.9}Ti_{0.1}O_9$ (SLBTT) were prepared by the molten salt approach successfully. The simultaneous substitution of La^{3+} and Ti^{4+} cause a decrease to a smaller cell volume, leading to a greater structural distortion. This in turn causes an increase in the dielectric constant, ferroelectric transition temperature, ferroelectric polarization and optical bandgap. The diffused phase transition (DPT) behavior is more pronounced in SLBTT exhibited by a broader dielectric peak without the frequency-dispersive behavior, primarily due to the increasing structural disorder of the *A*-site and *B*-site cations. The present work highlights the simultaneous substitution of *A*- and *B*-site cations is one of the most effective ways to obtain a pronounced ferroelectric material with a higher transition temperature.

Declaration of competing interest

The authors declare that they have no known competing financial interests or personal relationships that could have appeared to influence the work reported in this paper.

Acknowledgement

This work was financially supported by Universitas Andalas with project grant number: T/7/UN.16.17/PP/IS-PDU-KRP2GB-Unand/LPPM/2021.

References

[1] L. Yang, X. Kong, F. Li, H. Hao, Z. Cheng, H. Liu, J.F. Li, S. Zhang, Perovskite lead-free dielectrics for energy storage applications, Prog. Mater. Sci. 102 (2019) 72–108, https://doi.org/10.1016/j.pmatsci.2018.12.005.
[2] W. Gao, Y. Zhu, Y. Wang, G. Yuan, J.M. Liu, A review of flexible perovskite oxide ferroelectric films and their application, J. Mater. 6 (2020) 1–16, https://doi.org/10.1016/j.jmat.2019.11.001.
[3] H. Wei, H. Wang, Y. Xia, D. Cui, Y. Shi, M. Dong, C. Liu, T. Ding, J. Zhang, Y. Ma, N. Wang, Z. Wang, Y. Sun, R. Wei, Z. Guo, An overview of lead-free piezoelectric materials and devices, J. Mater. Chem. C. 6 (2018) 12446–12467, https://doi.org/10.1039/c8tc04515a.
[4] Y. Wang, X. Zhang, C. Zhang, R. Li, Y. Wang, C. Fan, Novel Bi4Ti3O12 hollow-spheres with highly-efficient CO2 photoreduction activity, Inorg. Chem. Commun. 116 (2020) 107931, https://doi.org/10.1016/j.inoche.2020.107931.
[5] A. Axelsson, F. Le Goupil, M. Valant, N.M. Alford, Electrocaloric effect in lead-free Aurivillius relaxor ferroelectric ceramics, Acta Mater. 124 (2017) 120–126, https://doi.org/10.1016/j.actamat.2016.11.001.
[6] B. Aurivillius, Mixed bismuth oxides with layer lattices 1. The structure type of CaNb2Bi2O9, Ark. För Kemi. 1 (1949) 463–480.
[7] H. Amorín, V.V. Shvartsman, A.L. Kholkin, M.E.V. Costa, Ferroelectric and dielectric anisotropy in high-quality SrBi2Ta2O9 single crystals, Appl. Phys. Lett. 85 (2004) 5667–5669, https://doi.org/10.1063/1.1836017.
[8] P. Fang, C. Zhi, Z. Xi, W. Long, X. Li, Cerium induced larger lattice distortion and piezoelectric properties of Aurivillius oxide Na0.25K0.25Bi2.5Nb2O9, J. Alloys Compd. 765 (2018) 848–853, https://doi.org/10.1016/j.jallcom.2018.06.127.
[9] T.P. Wendari, S. Arief, N. Mufti, A. Insani, J. Baas, G.R. Blake, Zulhadjri, Structure-property relationships in the lanthanide-substituted PbBi2Nb2O9 Aurivillius phase synthesized by the molten salt method, J. Alloys Compd. 860 (2021) 158440, https://doi.org/10.1016/j.jallcom.2020.158440.
[10] J. Yuan, R. Nie, Q. Chen, D. Xiao, J. Zhu, Structural distortion, piezoelectric properties, and electric resistivity of A-site substituted Bi3TiNbO9-based high-temperature piezoceramics, Mater. Res. Bull. 115 (2019) 70–79, https://doi.org/10.1016/j.materresbull.2019.03.019.
[11] Z. Zulhadjri, A.A. Billah, T.P. Wendari, E. Emriadi, U. Septiani, S. Arief, Synthesis of aurivillius phase CaBi4Ti4O15 doped with both La3+ and Mn3+ cations: crystal structure and dielectric properties, Mater. Res. 23 (2020) 2–6, https://doi.org/10.1590/1980-5373-MR-2019-0521.
[12] P. Sun, H. Wang, X. Bu, Z. Chen, J. Du, L. Li, F. Wen, W. Bai, P. Zheng, W. Wu, L. Zheng, Y. Zhang, Enhanced energy storage performance in bismuth layer-structured BaBi2Me2O9 (Me = Nb and Ta) relaxor ferroelectric ceramics, Ceram. Int. 46 (2020) 15907–15914, https://doi.org/10.1016/j.ceramint.2020.03.139.

[13] P. Banerjee, A.F Jr., Role of higher valent substituent on the dielectric and optical properties of Sr0.8Bi2.2Nb2O9 ceramics, Mater. Chem. Phys. 225 (2019) 213–218, https://doi.org/10.1016/j.matchemphys.2018.12.075.
[14] B.A. Hunter, Rietica - a Visual Rietveld Program, Australian Nuclear Science and Technology Organisation, Australia, 2000.
[15] S.L. Miller, R.D. Nasby, J.R. Schwank, M.S. Rodgers, P.V. Dressendorfer, Device modeling of ferroelectric capacitors, J. Appl. Phys. 68 (1990) 6463–6471, https://doi.org/10.1063/1.346845.
[16] Zulhadjri, T.P. Wendari, R. Ramadhani, Y.E. Putri, Imelda, La3+ substitution induced structural transformation in CaBi4Ti4O15 Aurivillius phases: synthesis, morphology, dielectric and optical properties, Ceram. Int. 47 (2021) 23549–23557, https://doi.org/10.1016/j.ceramint.2021.05.072.
[17] R.D. Shannon, Revised effective ionic radii and systematic studies of interatomie distances in halides and chaleogenides, Acta Crystallogr. 32 (1976) 751.
[18] H. Sun, Y. Lu, X. Xie, T. Yao, Z. Xu, Y. Wang, X. Chen, Structural, magnetic, and dielectric properties in Aurivillius phase Sr x Bi 6-x Fe 1-x/2 Co 1-x/2 Ti 3+x O 18, J. Eur. Ceram. Soc. 39 (2019) 2103–2110, https://doi.org/10.1016/j.jeurceramsoc.2018.12.060.
[19] Zulhadjri, T.P. Wendari, U. Septiani, S. Arief, Investigation on structure, dielectric and magnetic properties of the four-layer Aurivillius phase Pb1-xBi3.5+xNd0.5Ti4-xMnxO15 prepared via molten salt method, J. Solid State Chem. 292 (2020) 121723, https://doi.org/10.1016/j.jssc.2020.121723.
[20] Y. Shi, Y. Pu, J. Li, R. Shi, W. Wang, Q. Zhang, L. Guo, Structure, dielectric and multiferroic properties of three-layered aurivillius SrBi3Nb2FeO12 ceramics, Ceram. Int. 45 (2019) 9283–9287, https://doi.org/10.1016/j.ceramint.2019.01.129.
[21] D. Song, J. Yang, Y. Wang, Focus on the ferroelectric polarization behavior of four-layered Aurivillius multiferroic thin film, Ceram. Int. 45 (2019) 10080–10085, https://doi.org/10.1016/j.ceramint.2019.02.054.
[22] M. Zhang, X. Xu, Y. Yue, M. Palma, M.J. Reece, H. Yan, Multi elements substituted Aurivillius phase relaxor ferroelectrics using high entropy design concept, Mater. Des. 200 (2021) 109447, https://doi.org/10.1016/j.matdes.2020.109447.
[23] P. Nayak, K. Mitra, S. Panigrahi, Electrical and optical properties of four-layered perovskite ferroelectric ABi4Ti4O15(with A = Sr, Ba, Ca), Mater. Lett. 216 (2018) 54–57, https://doi.org/10.1016/j.matlet.2017.12.105.
[24] L.L. Zhang, Y.N. Huang, Theory of relaxor-ferroelectricity, Sci. Rep. 10 (2020) 1–18, https://doi.org/10.1038/s41598-020-61911-5.
[25] Z. Raddaoui, S. El Kossi, J. Dhahri, N. Abdelmoula, K. Taibi, Study of diffuse phase transition and relaxor ferroelectric behavior of Ba 0.97 Bi 0.02 Ti 0.9 Zr 0.05 Nb 0.04 O 3 ceramic, RSC Adv. 9 (2019) 2412–2425, https://doi.org/10.1039/c8ra08910h.
[26] Ismunandar, B.J. Kennedy, Effect of temperature on cation disorder in ABi2Nb2O9 (A = Sr, Ba), J. Mater. Chem. 9 (1999) 541–544, https://doi.org/10.1039/a806760k.
[27] Z. Yao, R. Chu, Z. Xu, J. Hao, G. Li, Enhanced electrical properties of (Li,Ce) co-doped Sr(Na0.5Bi0.5)Bi4Ti5O18 high temperature piezoceramics, RSC Adv. 6 (2016) 33387–33392, https://doi.org/10.1039/c6ra02203k.
[28] A. Amat, E. Mosconi, E. Ronca, C. Quarti, P. Umari, M.K. Nazeeruddin, M. Grätzel, F. De Angelis, Cation-induced band-gap tuning in organohalide perovskites: interplay of spin-orbit coupling and octahedra tilting, Nano Lett. 14 (2014) 3608–3616, https://doi.org/10.1021/nl5012992.